Journal of *Marine Science and Engineering*

MDPI

Article

Modelling of Sediment Transport and Deposition in Generating River-Mouth Closure: Oum-Errabia River, Morocco

Ismail Aouiche [1,*], Mouncef Sedrati [2] and Edward J. Anthony [3]

[1] Er-SHEMSS, Laboratory of Civil Engineering, Hydraulics, Environment and Climat, Hassania School of Public Works, Casablanca 20100, Morocco
[2] Geo-Ocean, Univ Bretagne Sud, Univ Brest, CNRS, Ifremer, UMR6538, F-56000 Vannes, France; mouncef.sedrati@univ-ubs.fr
[3] CNRS, IRD, INRAE, Coll France, CEREGE, Aix Marseille University, 13545 Aix-en-Provence, France; anthony@cerege.fr
* Correspondence: aouiche31@gmail.com

Abstract: River mouths are dynamic systems that can respond rapidly to both fluxes in fluvial water and sediment discharge and marine energy conditions, notably waves. On semi-arid wave-exposed coasts, the morphosedimentary behaviour of river mouths is particularly sensitive to variations in water discharge, which can be significantly influenced by climate variations, in addition to anthropogenic actions such as the construction of dams for water resource needs. In this climatic setting, an increasingly common consequence of decreasing river water discharge is the more or less prolonged closure of river mouths. Most studies have addressed river-mouth closure using analytical, parametric, numerical, or statistical models. The present study uses output from four numerical models to elucidate the hydrodynamic and sedimentary behaviour of the mouth of the Oum-Errabia River (catchment size: 35,000 km^2), which debouches on the Atlantic coast of Morocco. The historical evolution of the river mouth and the impact of human interventions, such as the construction of dams, are discussed. The study also briefly discusses the impact of the recent closure of the river outlet, in response to particularly low water discharge, on the marine ecosystem and water quality. The modelling results covering a one-year simulation in this situation of closure indicate a deposition of 427,400 m^3 of sediment in front of the mouth of the Oum-Errabia. Ensuring permanent river-mouth opening and tidal flushing and renewal of this river's estuarine waters will necessitate costly regular dredging.

Keywords: river mouth; hydrodynamics; sediment transport; river outlet closure; numerical modelling; river dams

Citation: Aouiche, I.; Sedrati, M.; Anthony, E.J. Modelling of Sediment Transport and Deposition in Generating River-Mouth Closure: Oum-Errabia River, Morocco. *J. Mar. Sci. Eng.* **2023**, *11*, 2051. https://doi.org/10.3390/jmse11112051

Academic Editor: Carl T. Friedrichs

Received: 29 September 2023
Revised: 23 October 2023
Accepted: 24 October 2023
Published: 26 October 2023

1. Introduction

The hydrodynamics and sedimentary behaviour of river mouths are jointly influenced by the river flow regime, wave climate, wind stress, tidal conditions, and anthropogenic actions materialized mainly by the construction of dams and ports [1,2]. In extreme cases of low flow, river mouths can be closed over more or less long periods of time (months to years), but episodic opening during high flood flow is also commonly observed (e.g., [3,4]). A common characteristic at river mouths in semi-arid to arid regions is the propensity for highly irregular flow regimes that may prompt river-mouth closure, as the relationship between water discharge and the wave conditions prevailing at the river mouth appears to be the paramount governing condition on this dynamic situation, although strong winds and changes in atmospheric pressure may also contribute in a non-negligible way but essentially in small estuaries (e.g., [5]). The term 'blind estuary' has been employed commonly in the literature to denote such small estuaries where low discharge conditions are conducive to semi-permanent closure (e.g., [4]). These sequences of opening and closure have important implications not only in terms of sediment management but also

from ecological and water-quality points of view (e.g., [6–8]). While these ecological considerations have attracted significant attention as a result of the importance of closure and opening on fish ecology in particular, little is known of the dynamics associated with the rapid changes that lead to closure and re-opening episodes. Even larger river systems than the commonly semi-permanently closed 'blind estuaries' evoked above can be forced into more or less long episodes of closure where the flow regime has been severely impacted by droughts or by anthropogenic actions. Recent studies on closure and opening have generally concerned small tidal inlets [9–12]. Most studies have addressed the closure of river mouths (and tidal inlets) using analytical solutions based on the equation of conservation of momentum [13], parametric models [14], numerical models [15,16]), or statistical models that link the state of the mouth or inlet solely with river flow [17,18]. Recent studies have predominantly focused on assessing pattern changes using high-resolution repeated multibeam surveys or employing numerical modelling of wave and current processes in isolation, without fully addressing the intricate numerical interactions that impact the morphological evolution of river-mouth closures. In our case study, the adopted numerical approach tracks morphological changes over the course of a year, taking into account the complex interplay among wave, current, tidal, and sediment transport processes, notably alongshore, with a one-hour hydrodynamic feedback loop.

The present study focuses on the hydrodynamic and sedimentary behaviour of the mouth of the Oum-Errabia River on the Atlantic coast of Morocco (Figure 1), which drains a relatively important catchment of 35,000 km^2. Following the construction of several dams, notably the Al Massira Dam at the end of the 1970s, the downstream flow at the river mouth dropped drastically, affecting the dynamics, morphology, and sedimentary behaviour of the mouth of the Oum-Errabia, with implications for ecosystem functioning and fluvial sediment supply to the adjacent coasts. Notwithstanding the fragmentation of the river by dams, the water discharge remained sufficiently high, however, to maintain permanent opening of the mouth. Over the last five years, however, the river mouth has progressively become clogged with sand, culminating in its closure at the end of the winter 2023, notwithstanding the fact that flood flows during the winter season commonly maintain a fairly wide outlet by dispersing sand. These changes are summarized in the satellite images in Figure 2, which cover nearly two decades.

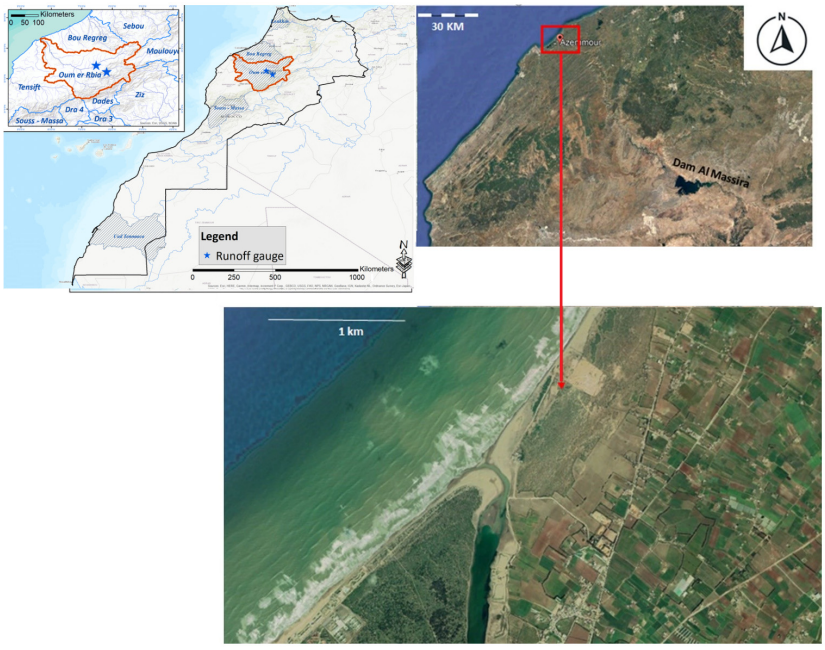

Figure 1. Location of the Oum-Errabia River catchment in the Middle Atlas Range in Central Morocco and the mouth of the river on the Atlantic Coast of Morocco (Atlas MTS and Google Earth, 2020).

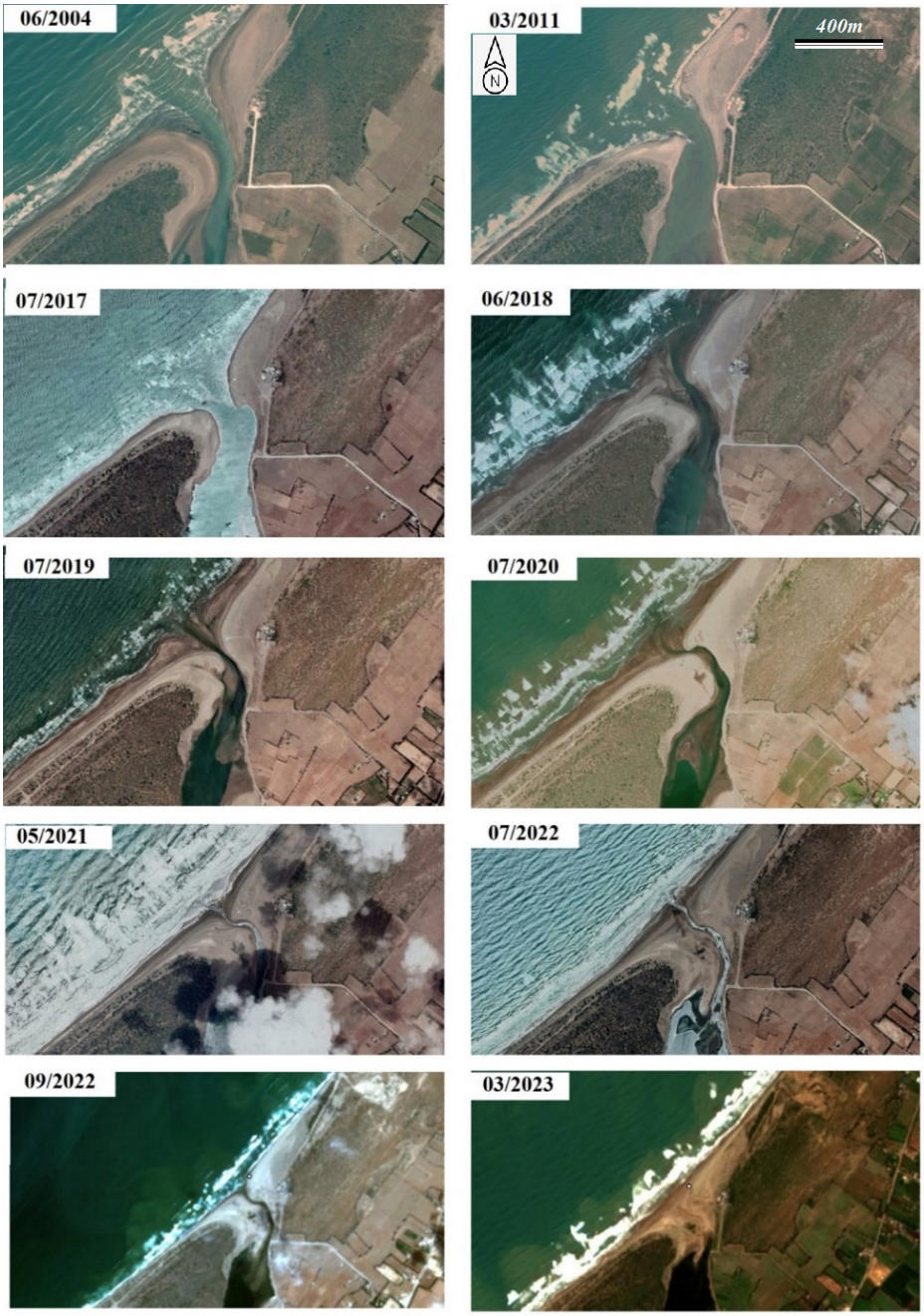

Figure 2. Morphological evolution of the Oum-Errabia River mouth from Geo-Eye satellite images showing progressive narrowing of the outlet from sand-clogging that has culminated in its closure in 2023.

Insight into the effects these changes have caused can be obtained by reconstructing the coastal sediment transport patterns and changes in the sediment budget at the mouth using coupled process modelling. To achieve this objective, we conducted a one-year simulation of waves and currents to document multiple patterns of shoreface change, from which we deduced sand transport pathways, the resultant alongshore sediment discharge, and a sediment budget. The study specifically examines the evolving conditions at the mouth of the Oum-Errabia River following the construction of dams, which have had a substantial impact on the flow dynamics. By examining this real-world case, we intend to elucidate the driving forces behind the recent mouth closure, following a historical situation of prevalence of an open outlet during the winter season. Our research takes a detailed look at the hydrodynamic and sedimentary responses to dam-induced flow alteration using

process modelling to decipher the sediment transport patterns and assess changes in the sediment budget. In this way, we endeavour to provide valuable insight into the causes and consequences of these transformations, shedding light on their implications for the estuarine ecosystem and river sediment supply to the coast.

2. The Oum-Errabia River and Its Mouth

The Oum-Errabia, formerly known as the Morbêa, is the second longest river in Morocco. The river debouches on the coast at the northern end of El Jadida Bay between the port of El Jadida and Cape Azemmour near the city of Azemmour (Figure 1). The river drains a catchment of 35,000 km^2 and has a length of 550 km and an average water discharge of 117 m^3/s. The Oum-Errabia has its sources in the Jebel Hayane near the rural settlement of Oum-Errabia at an altitude of 1800 m in the Middle Atlas range in central Morocco. The climate in this part of Morocco is of the Mediterranean type with both oceanic and continental influences. At the river catchment, the oceanic influence is associated with rainy winds from the Atlantic and the annual precipitation decreases, while the continental influence increases with distance from the sea. The latter influence results in high summer temperatures especially from June to August with a peak generally in July (around 41 °C in the mountains and 46 °C in the foothills) and relatively low winter temperatures from December to March (under −3 °C in the mountains and around 0 °C in the foothills) [19]. The Oum-Errabia's sediment transport capacity has been estimated at about 2400 m^3/year [20].

The Oum-Errabia catchment has experienced worrisome declines in surface water and groundwater resources, notably over the last few years. The catchment is now experiencing a deficit in rainfall for the fourth consecutive year since 2019. All the dams in this river basin, especially the Al Massira (Figure 1), have recorded low filling rates, averaging only 15%. The water resources stored in the various dams within the Oum-Errabia hydrographic basin from early September 2022 to the end of January 2023 reached approximately 372 million m^3, representing an estimated deficit of 62% compared to a normal year. The filling rate in 2023 does not exceed 8.5%, or approximately 420 million m^3, whereas it had reached around 10.3% during the same period in 2022, corresponding to approximately 509 million m^3 [20]. Future projections indicate that the hydrological dynamics in the upper portion of this watershed will be marked by a decrease in total flow, attributed to rising temperatures and declining precipitation [21,22]. Since the emergence of water scarcity at the Al Massira Dam, a consequence of both overexploitation and insufficient precipitation, there has been a notable reduction in dam releases. Consequently, the renewal of water within the Oum-Errabia estuary is primarily governed by tidal influx [20].

The beaches on either side of the river mouth consist of medium sand with a D50 of about 0.28 mm. These beaches exhibit a remarkably consistent cross-shore arrangement of morphological units consisting of a relatively straight 100 to 150 m wide foreshore and beachface bordering a vegetated dune ridge up to 800 m wide with embryonic border dunes present throughout. The upper shoreface is deficient in sand and characterized by a rocky substrate extending to a depth of −15 m offshore of the mouth of the Oum-Errabia. Below −15 m, a loose cover of fine bioclastic sand appears southwest of the Jorf Lasfar cliff, transitioning into accumulations of coarse terrigenous sand. A comprehensive survey of the entire coastal zone between the Oum-Errabia River mouth and the beaches located south of Cape Blanc shows this sand cover to be variably thick.

The prevailing winds in the region mainly originate from the west to southwest, north, and northeast sectors. Strong winds, ranging from 11 to 16 m/s, are typically experienced from the west and southwest directions. SIMAR 44 wave data provided by the Port Authorities of Spain (https://www.puertos.es/en-us/oceanografia/Pages/portus.aspx (accessed on 25 September 2023) using the WAM model show that over 80% of the swells originate from the NW and NNW directions. Swells with significant heights ranging from 1 m to 2.5 m and peak periods between 8 s and 11 s dominate, accounting for approximately

84% of the occurrences. Tides are semi-diurnal and have a mean range of approximately 2–3 m, attaining up to 4.48 m during spring tides [22].

3. Materials and Methods

In order to highlight the hydrodynamic processes and associated sediment dynamics, we use a combination of four modules of the MIKE 21 FM model (Danish Hydraulic Institute, 2020): a wave module (MIKE 21 SW), a hydrodynamic module (MIKE 21 HD), a sedimentary transport module (MIKE 21 ST), and a longshore transport module (MIKE 21 Shoreline Morphology). The model calculates waves, flows, sediment transport, and morphological evolution on an unstructured mesh and in a sequential and fully integrated manner (Danish Hydraulic Institute, 2022). The MIKE 21 FM model has been used extensively in the literature, providing realistic outputs of coastal morphological change [23–29].

Numerical models of coastal morphology simulate a variety of coastal processes, including wave generation and transformation, coastal circulation, and sediment transport. These models employ the principle of mass conservation to calculate changes in coastal morphology. To simulate these processes across the model domain, specific input forcings such as water elevation, discharge, and wave conditions are prescribed at the boundaries. In recent years, specific input reduction techniques have been developed to efficiently enable simulations of coastal morphological evolution over timescales ranging from years to decades [30–33]. These wave reduction techniques can be utilized for morphological modelling of most wave-dominated coastlines worldwide. However, morphological modelling has its limitations, and wave reduction techniques may not be the most suitable solution for all cases. For instance, in coastal segments characterized by a mild wave climate and where morphological changes are primarily driven by episodic major storms or areas with river mouths, the proposed methods are not readily applicable. In such regions, the use of a hybrid approach is recommended [34]. The hybrid approach adopted in our case involves utilizing the chronology-based wave/tide/wind input technique to enhance the accuracy of the modelling.

3.1. MIKE 21 SW

MIKE 21 SW is a state-of-the-art third generation spectral wind–wave model developed by the Danish Hydraulic Institute (DHI). The model simulates the growth, decay and transformation of wind-generated waves and swells in offshore and coastal areas. The fully spectral model MIKE 21 SW takes into account the following physical phenomena: wave growth under the action of wind, non-linear wave–wave interactions, dissipation due to white-capping, dissipation due to bottom friction, dissipation due to depth-induced wave breaking, refraction and shoaling due to depth variations, wave–current interactions, and the effect of time-varying water depth [35].

The governing equation in MIKE 21 is the wave action balance formulated in either Cartesian or spherical co-ordinates. In horizontal Cartesian coordinates, the conservation for wave action is given by:

$$\frac{\partial \mathrm{N}}{\partial t} + \nabla \cdot (\mathrm{VN}) = \frac{S}{\sigma}$$

where N ((x,y), s, ϴ, t) is the action density; t, the time, (x,y) the Cartesian co-ordinates; v(Cx, Cy, Cs, Cϴ), the wave group propagation in four-dimensional phase space; S, the source term for the energy balance; and V, the four-dimensional differential operator in ((x,y), s, ϴ) space. The source function term, S, on the right-hand side of the wave action conservation equation, is given by S = Sin + Snl + Sds + Sbot + Ssurf. Here, Sin represents the momentum transfer of wind energy to wave generation; Snl, the energy transfer due to non-linear wave, wave interaction; Sds, the dissipation of wave energy due to white capping (deep water wave breaking); Sbot, the dissipation due to bottom friction; and Ssurf, the dissipation of wave energy due to depth-induced breaking.

3.2. MIKE 21 HD

Hydrodynamic modelling is central in most modelling tasks in the marine area. Apart from being important in itself, it also forms the basis for a number of other tasks, such as sediment transport simulations. The hydrodynamic model (MIKE 21 HD) solves the equations for the conservation of mass and momentum as well as for salinity and temperature in response to a variety of forcing functions. The MIKE 21 HD module allows to specify a variety of hydrographic boundary conditions, initial conditions, bed resistance and wind forcing, etc.

MIKE 21 uses 2-D incompressible Reynolds-averaged Navier Stokes equations by accounting for the Boussinesq assumptions. The two-dimensional flow is solved by MIKE 21 HD with a double sweep algorithm technique. This means that the hydrodynamic module combines the mass balance equation and momentum conservation equation [36]. The following equations, the conservation of mass and momentum integrated over the vertical, describe the flow and water level variations. The local continuity equation is written as:

$$\frac{\partial u}{\partial x} + \frac{\partial v}{\partial y} + \frac{\partial w}{\partial z} = S$$

And the two horizontal momentum equations for the x- and y-component, respectively, are:

$$\frac{\partial \mathrm{u}}{\partial \mathrm{t}} + \frac{\partial \mathrm{u}^2}{\partial \mathrm{x}} + \frac{\partial \mathrm{vu}}{\partial \mathrm{y}} + \frac{\partial \mathrm{wu}}{\partial z} = f\mathrm{v} - \mathrm{g}\frac{\partial \eta}{\partial \mathrm{x}} - \frac{1}{\rho_0}\frac{\partial P_a}{\partial x} - \frac{g}{\rho_0}\int_z^n \frac{\partial \rho}{\partial x}\mathrm{d}z + F_u + \frac{\partial}{\partial z}\left(v_t \frac{\partial u}{\partial z}\right) + u_s S$$

$$\frac{\partial v}{\partial t} + \frac{\partial v^2}{\partial y} + \frac{\partial uv}{\partial x} + \frac{\partial wv}{\partial z} = -fu - g\frac{\partial \eta}{\partial y} - \frac{1}{\rho_0}\frac{\partial P_a}{\partial y} - \frac{g}{\rho_0}\int_z^n \frac{\partial \rho}{\partial x}\mathrm{d}z + F_v + \frac{\partial}{\partial z}\left(v_t \frac{\partial v}{\partial z}\right) + v_s S$$

In the hydrodynamic module, calculation of temperature (T) and salinity (S) transports follows the general transport diffusion equation as:

$$\frac{\partial T}{\partial t} + \frac{\partial uT}{\partial x} + \frac{\partial vT}{\partial y} + \frac{\partial wT}{\partial z} = F_T + \frac{\partial}{\partial z}\left(D_v \frac{\partial T}{\partial z}\right) + \hat{H} + T_s S$$

$$\frac{\partial s}{\partial t} + \frac{\partial us}{\partial x} + \frac{\partial vs}{\partial y} + \frac{\partial ws}{\partial z} = F_s + \frac{\partial}{\partial z}\left(D_v \frac{\partial s}{\partial z}\right) + s_s S$$

The horizontal diffusion terms are defined as:

$$(F_T, F_s) = \left[\frac{\partial}{\partial x}\left(D_h \frac{\partial}{\partial x}\right) + \frac{\partial}{\partial y}\left(D_h \frac{\partial}{\partial y}\right)\right](T, s)$$

The equations for two-dimensional flow are obtained by integration over depth: where x, y, and z are the Cartesian co-ordinates; u, v, and w, the flow velocity components; t, time; T and s, temperature and salinity, respectively; Dv, the vertical turbulent (eddy) diffusion coefficient; S, magnitude of discharge due to point sources; Ts and ss, temperature and salinity of the source; FT and Fs, the horizontal diffusion terms; Dh, the horizontal diffusion coefficient; and h, depth.

3.3. MIKE 21 ST and Morphological Restitution

MIKE 21 ST is an intra-wave sand transport model. The trajectories followed by sediments are a direct result of the currents generated by wind, waves, and tides. The ultimate goal is to quantitatively and qualitatively determine how sand is transported and deposited in the study area with the integrated wave boundary layer approach. The adopted method takes into account the hydrodynamic feedback over one year of simulation with a time step of 3 h. Integration of the sedimentary model enables the implementation of a morphological model, providing continuous feedback between hydrodynamic and sedimentological conditions. This method provides a realistic approach to the morphological evolution of the area. Sediment transport patterns around engineering structures or near tidal inlets or river outlets are calculated by coupling MIKE 21/3 Sand Transport with MIKE 21/3 Hydrodynamics and MIKE 21 Spectral Waves. Mike 21 ST is capable of

calculating transport rates under combined current and waves (breaking or unbroken) at arbitrary angles.

To ensure better estimates of the total longshore transport and to allow for more realistic feedback between the intertidal zone and the nearshore area, the hybrid model of Kaergaard and Fredsoe [37] is adopted. The approach we have adopted is original and consists combining a spectral wave model, a hydrodynamic model, a sediment transport model, and a cross-shore integration method of longshore transport to estimate the net flux of sediment transported for each longshore portion of the beach. The calculation grid consists of an unstructured mesh with finite volumes, which are obtained by iteratively propagating the shape of the coastline seaward using a specific technique (see Figure 3).

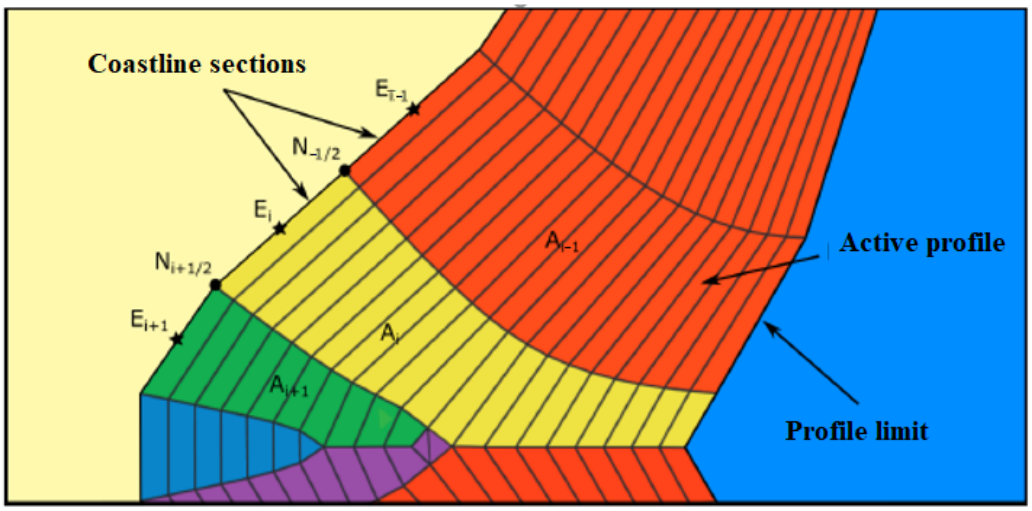

Figure 3. Example of an unstructured grid used in the Kaergaard and Fredsoe model (2013a) to determine the beach area (Ai) associated with each stretch of coastline (Ei). Adapted from Kaergaard and Fredsoe (2013a).

This feature provides access to the active surface associated with each portion of the coast, which ensures a good correspondence between the volumes of accumulated or eroded sediment and the variations in the position of the coastline. The use of a system of local coordinates following the orientation of the coastline allows the model to correctly simulate the evolutions of coastlines having a strong curvature and to manage the existence of multiple plan positions of the coastline. This model has proven capable of reproducing the development of various coastal features ranging from ripples to sandy spits, e.g., [38,39].

3.4. Model Set-Up

Simulations were conducted using representative wave climates over 1 year, taking into consideration the influence of tide and wind (Figure 4). Irregular (JONSWAP spectra), directional waves were applied at the offshore boundary of the MIKE 21 SW model. Default values were used for the wave breaking coefficients, with a constant gamma value of 0.8. Lateral boundaries were assumed to be symmetrical, in order to properly represent open-coast conditions. Radiation stresses, calculated by the wave module, were used to drive the longshore current in the HD module. Lateral boundary conditions (levels along and fluxes across shore-normal boundaries of the HD model) were generated using the radiation stresses calculated by MIKE 21 SW as input. Smagorinsky's formula with a coefficient equal to 0.28 was used to compute the velocity-based eddy viscosity [40].

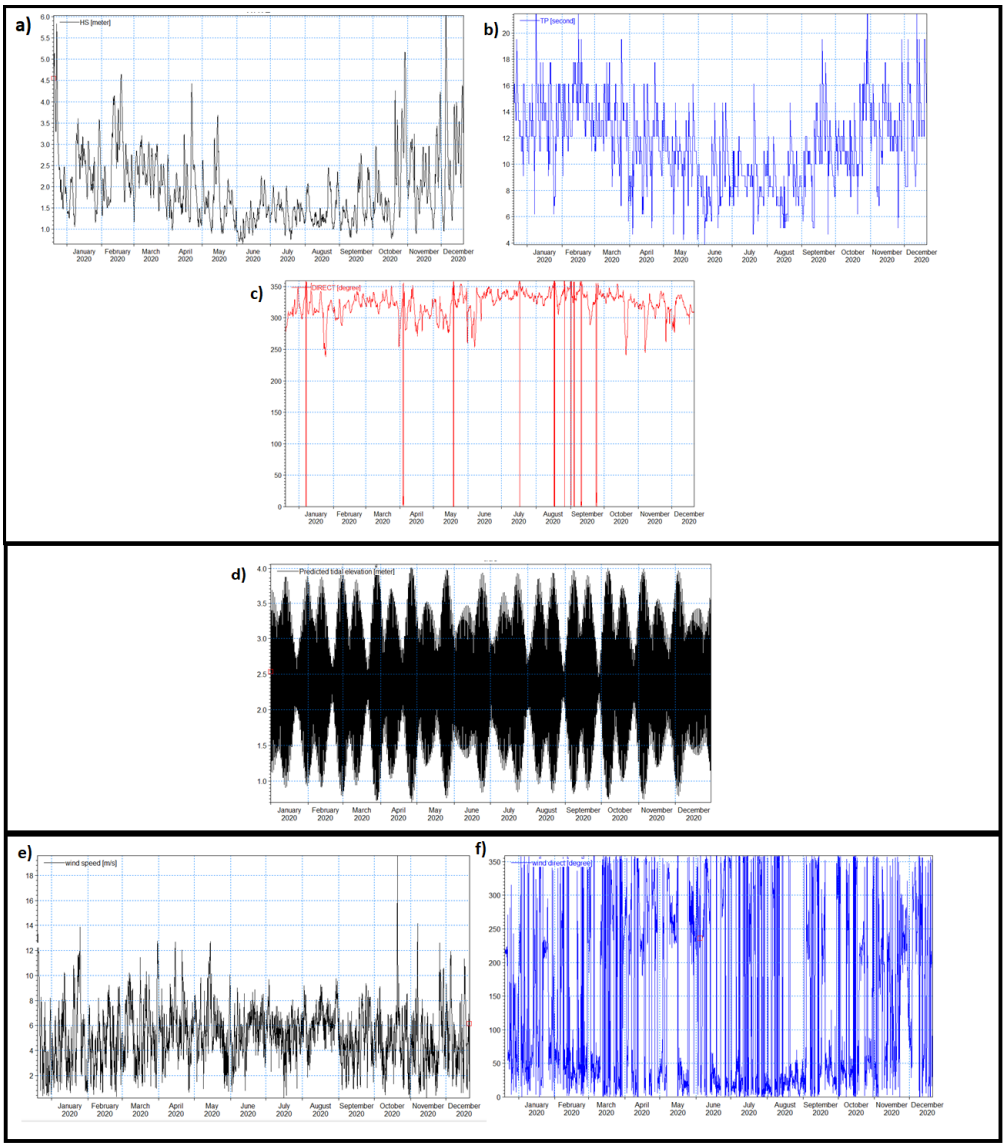

Figure 4. Annual cycles of wave, tide, and wind. (**a**) Significant wave heights (m); (**b**) peak periods of waves (s); (**c**) mean wave direction (°N); (**d**) water surface elevations due to tides (m); (**e**) wind speeds (m/s); (**f**) mean wind directions (°N).

The bathymetry in front of the mouth of the Oum-Errabia was condensed from a survey carried out in Mars 2020. The analysis of seabed changes was conducted from the bathymetric minutes, the use of which helps limit the error margins in bathymetric mapping [41]. The bathymetric map consisted of 53,000 points covering an area of 5.3 km^2, with a sounding every 10 m. We condensed the data to extract digital depth models [42] based on kriging, which as demonstrated by several authors [43–46] is the most appropriate method for digital depth model construction.

Model bathymetries were created on the basis of the survey carried out in 2020 using triangulation (Figure 5). Maps of bed roughness were defined based on sediment samples collected at the field sites (Nikuradse's roughness for SW and Manning number for HD module). Sediment samples collected were used for the sediment grain size distribution in the model. The median grain size (D50) varied between 0.2 and 0.3 mm.

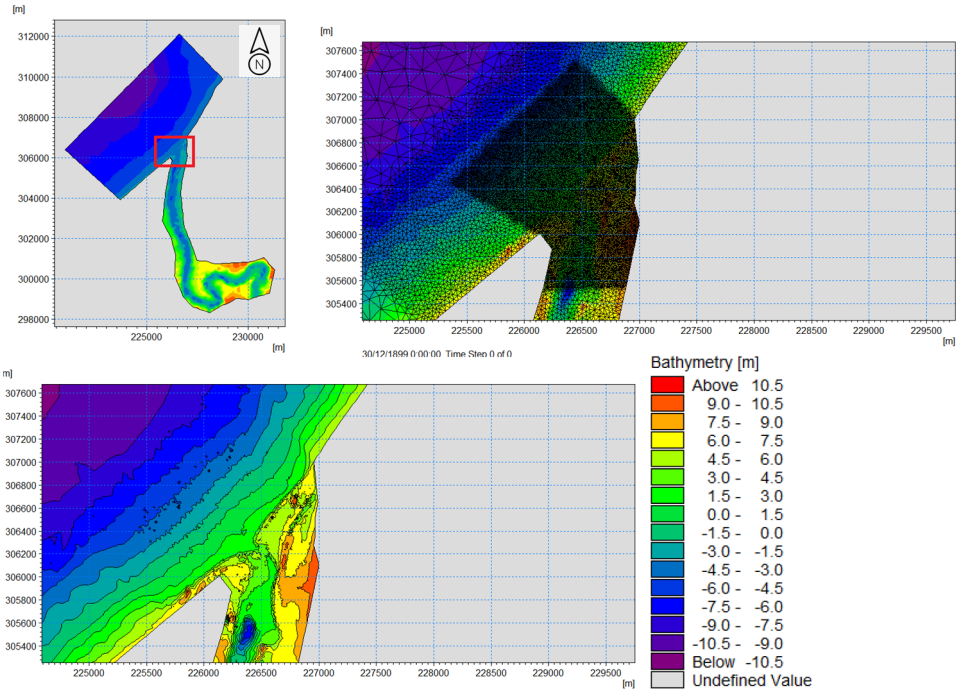

Figure 5. Hydrodynamic computational mesh and bathymetry of the mouth of the Oum-Errabia River.

To carry out our wave and current simulations and illustrate wave propagation from the outer continental shelf (depth 100 m) to the inner shoreface of the study area, we used the SIMAR 44 data (https://www.puertos.es/en-us/oceanografia/Pages/portus.aspx (accessed on 25 September 2023)). The simulated swell (see above), wind, and tide cycles employed in the model are illustrated below. Regarding the wind data, predominant W, N, and NNE directions are observed, with an average moderate speed of around 6.7 m/s. To ensure an accurate representation of tide-induced water level fluctuations, a comprehensive astronomical tidal cycle is incorporated as a boundary condition in the model. This tidal cycle integrates neap tide, spring tide, and mean tide components.

The modelling system used in this study consists of two domains: the larger one with a coarser mesh extending offshore of the study area and a finer-mesh domain covering the river outlet (Figure 5). The calculations are implemented using a flexible mesh for wave propagation and currents.

4. Results

4.1. Simulation of Wave Propagation

The simulation results of wave propagation demonstrate a deformation of the incoming waves from the NW and NNW, due to refraction. The Figure 6 below provides an example of the variation in the significant height of the swell. During all swell conditions, a significant break of the swell is observed at the outlet. Note that the location of this breaking zone varies with the tidal cycle. It occurs at the lower foreshore during neap tides and at the upper foreshore during spring tides. For more details, see animation in the link [https://drive.google.com/file/d/1_T9-wM1EYv4fMaAh5odJlJP80NMBoGKL/view?usp=sharing] (accessed on 25 September 2023)).

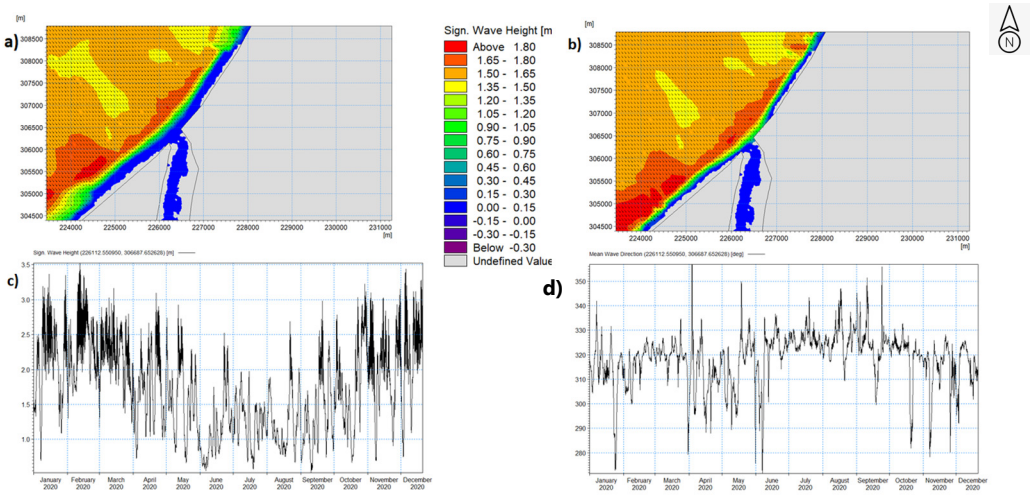

Figure 6. Wave characteristics in front of the mouth of the Oum-Errabia: (**a**) map of significant wave heights during low tides (time step = 711—matching the date of 29 March 2020, at 9:00 P.M.—low tide); (**b**) map of significant wave heights during high tides (time step = 709—matching the date of 29 March 2020, at 3:00 P.M.—high tide); (**c**) significant wave heights in front of the Oum-Errabia outlet; (**d**) mean wave direction in front of the Oum-Errabia outlet.

4.2. Simulation of the Water Surface Elevations

Throughout the simulation period, combining the effects of the tide, swell, and wind, the maximum water level variation within the river estuary is around 0.5 m; this value is recorded during spring tides when the tidal water level is above 3.6 m/Zh (Figure 7. The figures below present a comparison between the water level variations inside the estuary and those offshore. For more details, see the animation in the link. [https://drive.google.com/file/d/1vXLaUMLqTIqRVxi90j37wtnVRxvKwE_8/view?usp=sharing].

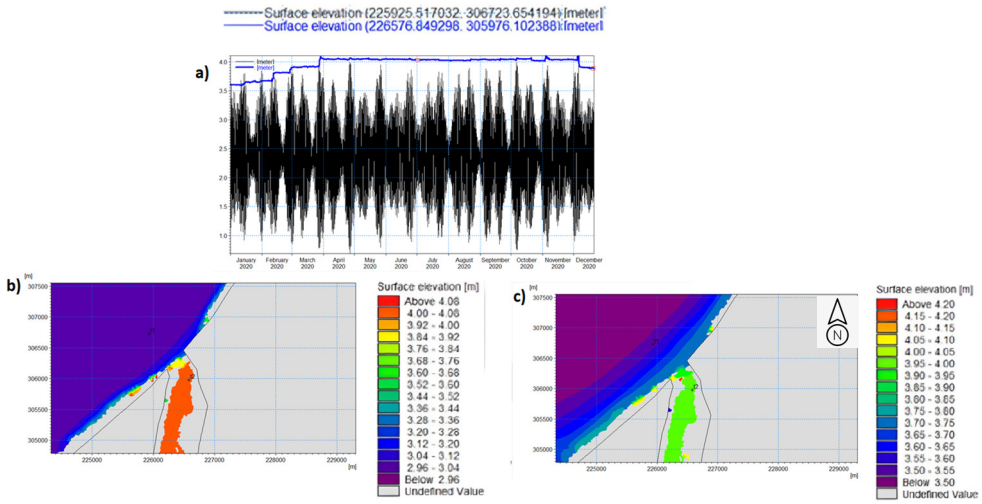

Figure 7. Water level variation outside and inside the mouth of the Oum-Errabia: (**a**) water levels over one year (blue line: inside the mouth, black: outside); (**b**) water levels resulting from the effects of swell/wind during neap tides—time step 701—matching the date of 28 March 2020, at 3:00 PM—high tide; (**c**) water level resulting from the effects of swell/wind during neap tides—time step 2723—matching the date of 9 December 2020, at 9:00 PM—high tide. For more details, see the animation in the link above.

Throughout the year, the volume of water oscillating between the estuary and the Atlantic Ocean is almost nil. Low levels of water exchange occur when high swell and strong wind conditions coincide with high tides in March, April, October, November, and

December (Figure 8). The flow in the course of these exchanges fluctuates between 1 and 9 m^3/s, with an average value of 0.036 m^3/s.

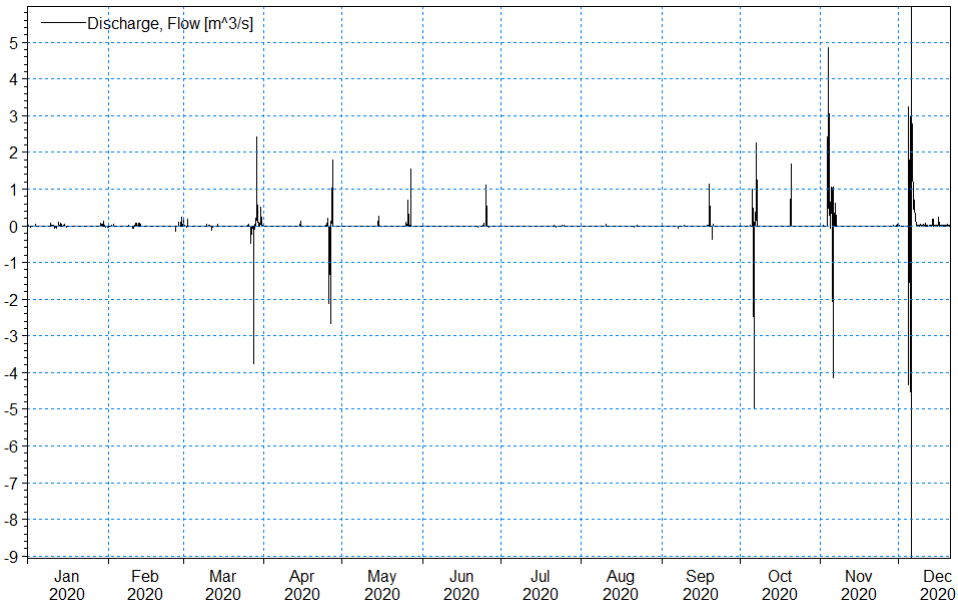

Figure 8. Simulation of river water discharge (m^3/s) at the mouth of the Oum-Errabia River. Negative values indicate discharge direction from the sea towards the estuary during the flood tide, while positive values indicate discharge flowing from the estuary towards the sea during the ebb tide. This exchange occurs only during significant high tides, exceeding approximately 4.0 m/ZH.

4.3. Simulation of Currents

The simulation of currents in the breaking zone has allowed for the characterization of radiation stress and the resolution of the Saint Venant equation. The radiation stress is defined as the excess momentum flux due to the presence of swell. The computed current vectors show the predominance of currents parallel to the coast (Figure 9). For more details, see animation in the link [https://drive.google.com/file/d/1hJqCo-w8lCbUwSKF7rTY9QAa08i4-5k9/view?usp=sharing].

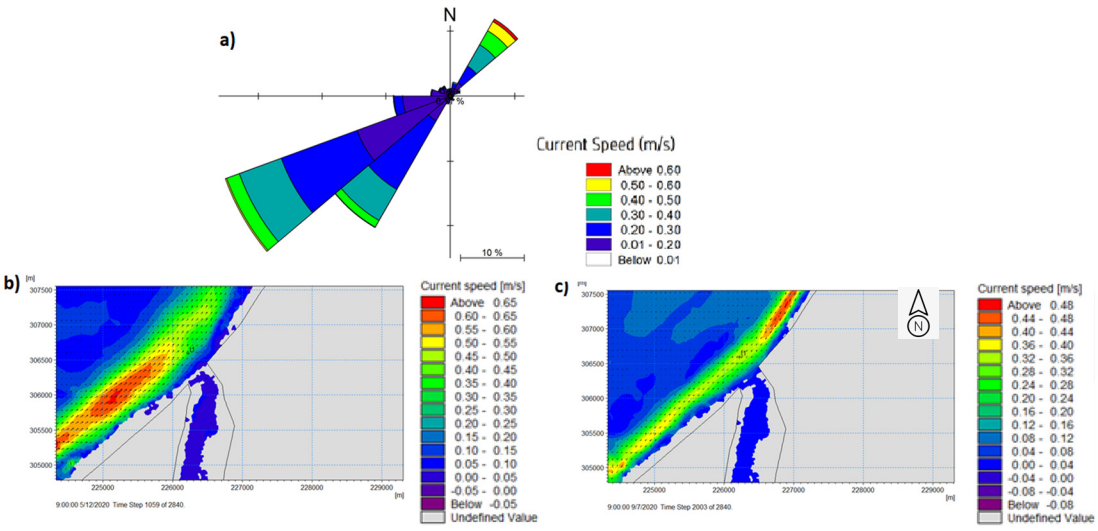

Figure 9. Current characteristics in front of the Oum-Errabia outlet: (**a**) current rose; (**b**) current speed, oriented SSW-NNE, time step 1059—matching the date of 12 May 2020, at 9:00 PM; (**c**) current speed, oriented NNE-SSW, time step 2003—matching the date of 7 September 2020, at 9:00 PM.

The currents flowing in a south-southwest direction have an occurrence rate of 85%, the remaining 15% being associated with north-northeast currents. However, it should be noted that despite the low occurrence rate of the latter currents, their speeds are significant (Figure 9), ranging in front of the outlet from 0.02 to 0.65 m/s, with an average value of 0.232 m/s.

4.4. Simulation of Sediment Transport

Simulations of sediment transport capacity exhibit an alternation between two drift directions, one oriented SSW-NNE with swells originating at 280–300 °N and the other NNE-SSW with swells from 330–360 °N, and additionally, a convergence of currents for swells originating at 300–330 °N (Figure 10). This two-drift regime promotes sediment deposition at the mouth of the Oum-Errabia River. See animation in the link: https://drive.google.com/file/d/1Pth1oyj6i_EbsYpN_US3UYiUcwO1HfJ2/view.

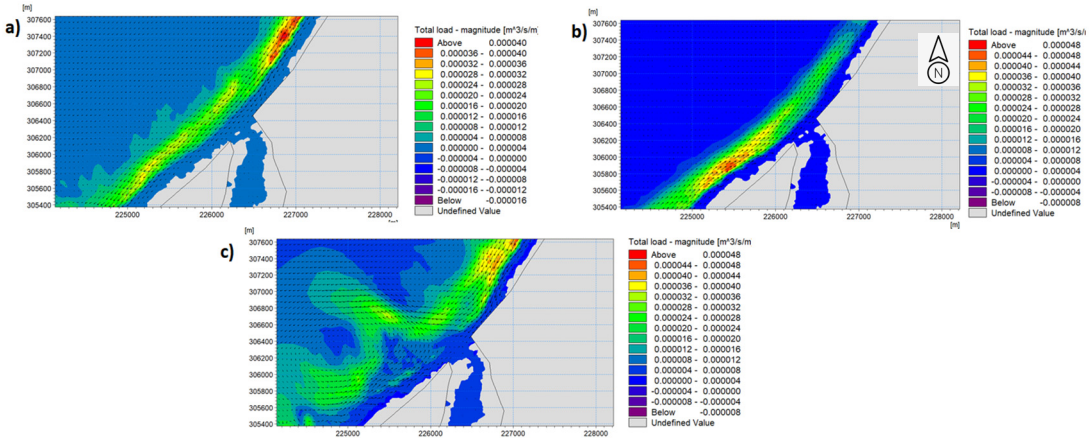

Figure 10. Sediment transport capacity in front of the Oum-Errabia outlet: (**a**) total sediment load (m^3/s per m of shoreline) associated with waves from 330–360 °N; (**b**) total sediment load (m^3/s per m of shoreline) associated with waves from 280–300 °N direction; (**c**) total sediment load (m^3/s per m of shoreline) associated with waves from 300–330 °N.

To determine the net sediment transport capacity, two profiles perpendicular to the coast are used to define the outlet area of the Oum-Errabia (Figure 11).

- Profile 1, situated north of the outlet, exhibits a NNE-SSW dominant direction with a drift potential that ranges from −0.053 to +0.32 m^3/s, whereas profile 2, located south of the outlet, displays a SSW-NNE dominant direction with a drift varying from −0.17 to 0.11 m^3/s (Figure 11a,b).
- The cumulative sediment transport results reveal that the Oum-Errabia outlet is dominated by net drift, oriented NNE-SSW, that results in the deposition of approximately 349,240 m^3/year of sediment and an associated net secondary drift, oriented SSW-NNE, that leads to deposition of around 78,188 m^3/year. In total, 427,428 m^3/year of sediment are deposited in front of the Oum-Errabia outlet (Figure 11c,d).

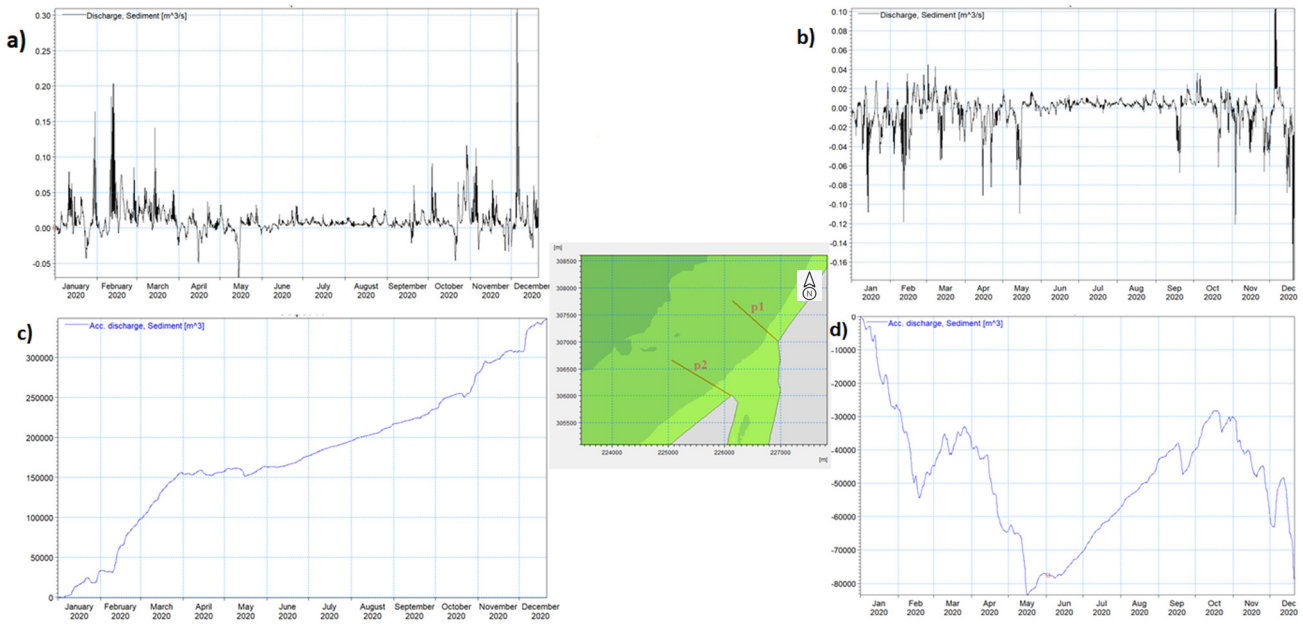

Figure 11. Net sediment transport capacity in front of the Oum-Errabia outlet: (**a**) sediment load in transit at profile 01 (m^3/s); (**b**) sediment load in transit at profile 02 (m^3/s); (**c**) net sediment load in transit at profile 01 (m^3); (**d**) net sediment load in transit at profile 01 (m^3). The negative sign indicates SSW-NNE sediment transport and the positive sign, NNE-SSW transport.

Figure 12 depicts the bed-level changes following 365 days of simulation, validating the previous results that showed the presence of deposition in the form of a bar in front of the mouth of the Oum-Errabia. For further details, please refer to the animation provided in the following link: [https://drive.google.com/file/d/1Hk38ADMlFOjiDKBz8QCkOtVQQcRpmIST/view?usp=sharing].

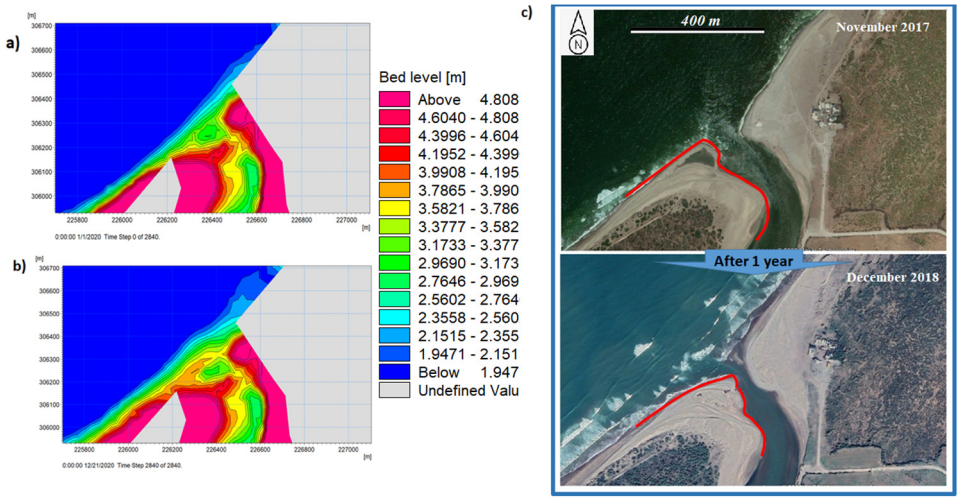

Figure 12. Bed-level change following 365 days of simulation: (**a**) bed level at the beginning of the simulation; (**b**) bed level at the end of the simulation—after 365 days. The numerical bed-level evolution demonstrates the mobility of the sediment mass located at the southwest of the estuary mouth. Satellite image (**c**) depicting clear convergence between the overall plan-view closure trends and bed-level patterns yielded by the numerical simulations.

5. Discussion

Following several decades of anthropogenic modification of its catchment during which the mouth of the Oum-Errabia River maintained an open outlet, closure now pre-

vails. This situation is related to the deterioration of the water discharge level of the river, a situation that in turn reinforces the action of waves on the outlet morphology, notwithstanding the relatively large size of the Oum-Errabia catchment. This shows the importance of high discharge in maintaining outlet opening in semi-arid regions. Sediment accumulation in the vicinity of river mouths is a classic condition associated generally with localized wave refraction and dissipation effects related to the interaction between fluvial water and bedload discharge and incident waves, and this generates distinct sediment cells [47–49]. The local sediment cell system in front of river mouths is generally embedded in a longshore transport system that can be either quasi-permanently unidirectional such as at the mouth of the large Senegal river delta [50] or bi-directional with alternations in the transport direction as a function of wave direction that may change at scales ranging from days to seasonal or even longer as with ENSO cycles, as in the cases of the Souss (catchment size: 22,000 km^2) and Massa (catchment size: 4900 km^2) located further south on the Moroccan coast [23,51]. The bi-directional longshore transport system that prevails on this part of the Moroccan coast and evidenced by the modelling results (Figure 10) was hitherto characterized by sediment bypass, either to the north across the mouth or to the south, with river flushing assuring outlet stability. A one-year numerical simulation of the hydrodynamics and sediment transport at the mouth of the Oum-Errabia River shows a transport convergence in front of the river's outlet characterized by the accumulation of a significant volume of sand on the foreshore and inner shoreface. This two-drift regime promotes sediment deposition at the outlet of the Oum-Errabia. Deposition can be reinforced both by morphological feedback as the amount of sediment accumulating increases, inducing further dissipation of wave energy and longshore currents and weakening of the fluvial jet due to reduction in river discharge, which diminishes the sediment reworking capacity of the outflow.

Given the significant water requirements that need to be met upstream in the Oum-Errabia watershed, the river's discharge downstream of the Al Massira Dam has been dwindling over the last ten years. These conditions have been further exacerbated by a degradation of the climate conditions in the catchment, associated with a notable drop in rainfall [21] and river discharge and a significant lowering of the storage capacity of the Al Massira Dam (Figure 13). These conditions progressively weakened the water and sediment flushing capacity of the river at its mouth, leading to degradation of the sanitary conditions and ecology of the estuary. As river discharge diminished, the estuary progressively lost its capacity to ensure flushing and water renewal. The outlet closure that finally occurred in 2023 now implies that the estuary's capacity to flush water, sediments and pollutants is virtually nil, leading to a degradation of estuarine ecological functions. This deterioration aspect of water quality and its impact on resources, including estuarine, has been abundantly recognized in Morocco [6,7,52,53]. Water quality in the Oum-Errabia estuary has been further degraded by the impounding of untreated wastewater discharged by collectors in the city of Azzemour (Figure 1) and its surroundings, a situation that is generating serious levels of pollution. The permanent closure of the mouth of the Oum-Errabia is, no doubt, also having detrimental effects on the marine ecosystem.

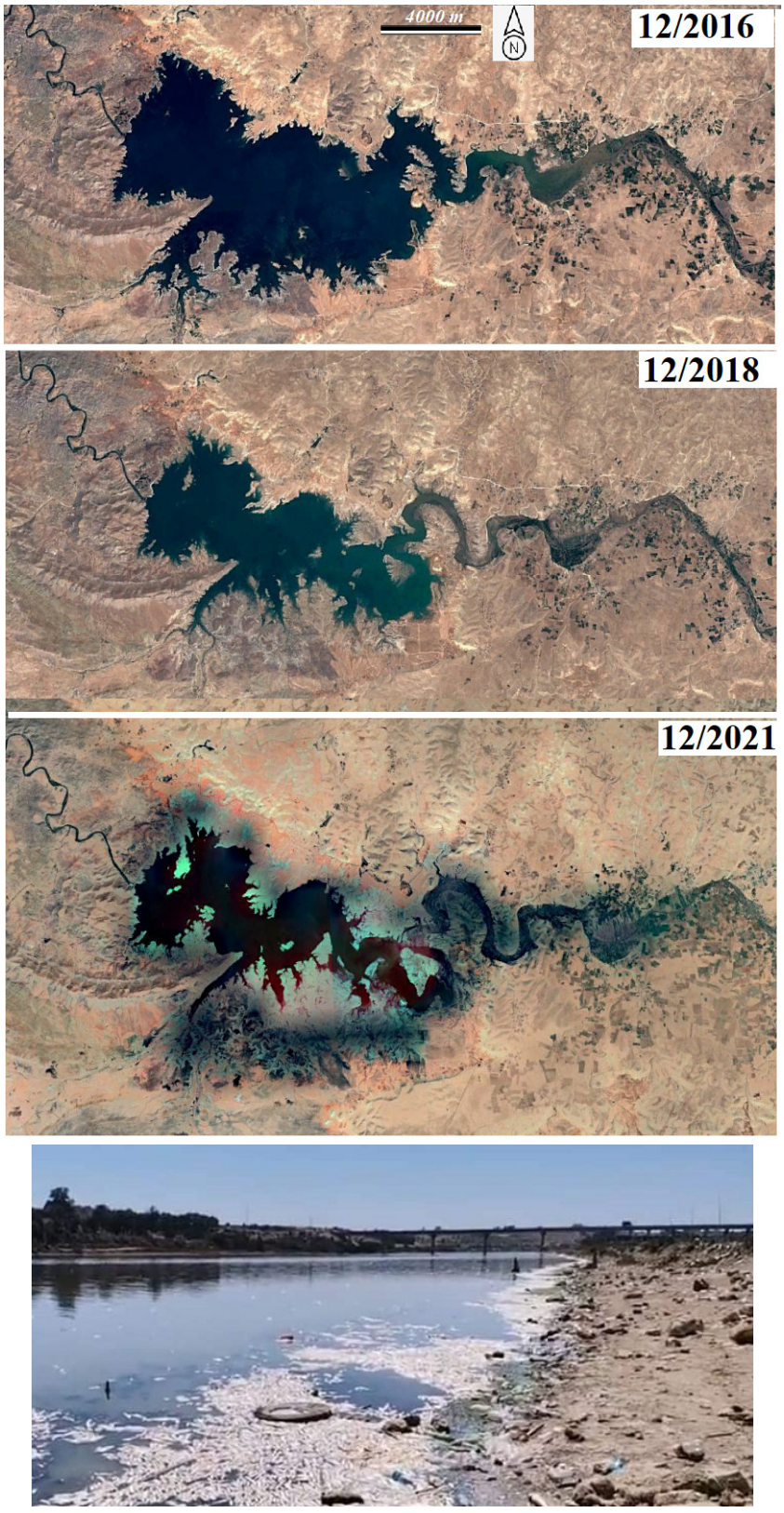

Figure 13. Geo-Eye satellite images showing the drastic decrease in water level at the Al Massira dam since 2018, and 2023 ground photograph near the mouth of the Oum-Errabia depicting marked pollution associated with the degradation of water quality related to both the drop in water discharge and blocking of flushing as a result of mouth closure.

The current fate of the mouth of the Oum-Errabia River is similar to that of several other river outlets of small to moderate-sized catchments (up to 50,000 km^2) in Morocco such as the Ksob [54] and the Massa [51], but also in the Mediterranean [51,55].

The Moroccan port authorities have now embarked on conducting parallel studies to monitor the evolution of the Oum-Errabia River estuary in order to prevent its complete closure. If left unrectified, the closure of the outlet will inevitably result in eutrophication of the estuarine waters, causing further pollution. It is estimated that an annual dredging of 427,428 m^3 is necessary to maintain the river mouth open. However, given the longshore drift capacity along the coast, closure could occur rapidly during winter storms (November through March), with the rapid accumulation of up to 300,000 m^3 of sand. Unless the river's water discharge is raised to the levels it had in the 1980s and 1990s, the closure of its outlet will become recurrent, in spite of dredging. The future appears rather bleak, as we grapple with the compounding challenges of increasing water demands in the catchment area and diminishing rainfall associated with climate change [19,21].

6. Conclusions

In this study, we show that the closure of the outlet of the Oum-Errabia River can be explained as a combined response to processes acting at different timescales. We also show the need to take into consideration all physical phenomena acting on the outlet environment in order to better understand its morphological evolution, and combine this with a modelling approach in predicting future trends. The river's outlet has experienced significant sedimentation and closure due to both natural and anthropogenic factors. The river flow has been impaired by dams, and water quality degraded by wastewater discharged without treatment. By annihilating the water and sediment flushing capacity of the river, outlet closure and the consequent increase in pollution, in what has now become a 'blind estuary', jeopardize the estuarine and marine ecosystem. Understanding the hydrodynamics and associated sedimentary behaviour of this system, through both modelling and field-based observations, is necessary in order to successfully identify the sources of these problems, manage the impacts of human interventions, and emplace mitigation and rehabilitation measures.

Author Contributions: Writing—Original Draft, I.A.; Supervision, M.S.; Validation, E.J.A. All authors have read and agreed to the published version of the manuscript.

Funding: This research received no external funding.

Institutional Review Board Statement: Not applicable.

Informed Consent Statement: Not applicable.

Data Availability Statement: Not applicable.

Acknowledgments: We thank the two reviewers for their constructive suggestions.

Conflicts of Interest: The authors declare no conflict of interest.

References

1. Mount, J.F. *California Rivers and Streams: The Conflict Between Fluvial Processes and Land Use*; University of California Press: Berkeley, CA, USA, 1995; 376p.
2. Stretch, D.; Parkinson, M. The breaching of sand barriers at perched, temporary open/closed estuaries—A model study. *Coast. Eng. J.* **2006**, *48*, 13–30. [CrossRef]
3. Whitfield, A.K. A characterization of southern African estuarine systems. *South. Afr. J. Aquat. Sci.* **1992**, *18*, 89–103. [CrossRef]
4. Cooper, J.A.G. Geomorphological variability among microtidal estuaries from the wave-dominated South African coast. *Geomorphology* **2001**, *40*, 99. [CrossRef]
5. Barriocanal, C.; Crous, A.; Varga, D.; Vila, J. Preliminary assessment of factors responsible for periodic river mouth closure, River Daró, (Costa Brava, Girona). *J. Coast. Res.* **2006**, *48*, 16–20.
6. Gillson, J. Freshwater flow and fisheries production in estuarine and coastal systems: Where a drop of rain is not lost. *Rev. Fish. Sci.* **2011**, *19*, 168–186. [CrossRef]

7. Brito, A.C. A changing definition of estuary? *Adjusting concepts to intermittently closed and open coastal systems. J. Ecosyst. Ecography* **2012**, *2*, 1000–1006. [CrossRef]
8. Chavez-Lopez, R.; Rocha-Ramirez, A. Fish community composition from El Llano Lagoon blind estuary, Veracruz, Mexico. *Rev. Mex. Biodivers.* **2020**, *91*, e912494. [CrossRef]
9. Duong, T.M.; Ranasinghe, R.; Walstra, D.; Roelvink, D. Assessing climate change impacts on the stability of small tidal inlet systems: Why and how? *Earth-Sci. Rev.* **2016**, *164*, 369–380. [CrossRef]
10. Lam, N.T. Hydrodynamics and Morphodynamics of a Season-Ally Forced Tidal Inlet System. Ph.D. Dissertation, Delft University of Technology, Delft, The Netherlands, 2009; 126p.
11. Ranasinghe, R.; Duong, T.M.; Uhlenbrook, S.; Roelvink, D.; Stive, M. Climate-change impact assessment for inlet-interrupted coastlines. *Nat. Clim. Chang.* **2013**, *31*, 83–87. [CrossRef]
12. Tung, T.T. Morphodynamics of Seasonal Closed Coastal Inlets at the Central Coast of Vietnam. Ph.D. Dissertation, Delft University of Technology, Delft, The Netherlands, 2011.
13. Rustomji, P. Flood and drought impacts on the opening regime of a wave-dominated estuary. *Mar. Freshw. Res.* **2007**, *58*, 1108–1119. [CrossRef]
14. O'Brien, M.P. *Notes on Tidal Inlets on Sandy Shores*; GITI Report 5; U.S. Army Coastal Engineering Research Center (USACE): Washington, DC, USA, 1976; 27p.
15. Ranasinghe, R.; Pattiaratchi, C. Circulation and mixing characteristics of a seasonally-open tidal inlet: A field study. *J. Mar. Freshw. Res.* **1999**, *50*, 281–290. [CrossRef]
16. Ranasinghe, R.; Pattiaratchi, C. The seasonal closure of tidal inlets: Wilson Inlet—A case study. *Coast. Eng.* **1999**, *37*, 37–56. [CrossRef]
17. Elwany, M.H.S.; Flick, R.E.; Aijaz, S. Opening and closure of a marginal southern California lagoon inlet. *Estuaries* **1998**, *21*, 246–254. [CrossRef]
18. Walker, D. Assessing environmental flow requirements for a river-dominated tidal inlet. *J. Coast. Res.* **2003**, *19*, 171–179.
19. Ouatiki, H.; Boudhar, A.; Tramblay, Y.; Jarlan, L.; Benabdelouhab, T.; Hanich, L.; El Meslouhi, M.; Chehbouni, A. Evaluation of TRMM 3B42 V7 Rainfall Product over the Oum Er Rbia Watershed in Morocco. *Climate* **2017**, *5*, 1. [CrossRef]
20. ABHOER (Agence du Bassin Hydraulique de l'Oum Er-Rbia) "Monthly Report of Dam Levels 2023. Available online: https://data.gov.ma/fr/feedback/situation-journaliere-des-principaux-grands-barrages (accessed on 25 September 2023).
21. Ouatiki, Y.; Boudhar, A.; Ouhinou, A.; Arioua, A.; Hssaisoune, M.; Bouamri, H.; Benabdelouahab, T. Trend analysis of rainfall and drought over the Oum Er-Rbia River Basin in Morocco during 1970–2010. *Arab. J. Geosci.* **2019**, *12*, 128. [CrossRef]
22. Chaïbi, M.; Sabatier, F. Budget sédimentaire du littoral de la baie d'El Jadida (Maroc). *Méditerranée* **2010**, *115*, 116–124. [CrossRef]
23. Aouiche, I.; Daoudi, L.; Anthony, E.J.; Sedrati, M.; El Mimouni, A.; Dussouillez, P. Alongshore variations in morphology and incident wave energy on a human-impacted coast: Agadir, Morocco. *J. Coast. Res.* **2016**, *2*, 1027–1031. [CrossRef]
24. Aouiche, I.; Daoudi, L.; Anthony, E.J.; Sedrati, M.; Ziane, E.; Harti, A.; Dussouillez, P. Anthropogenic effects on shoreface and shoreline changes: Input from a multi-method analysis, Agadir Bay, Morocco. *Geomorphology* **2016**, *254*, 16–31. [CrossRef]
25. Aouiche, I.; Daoudi, L.; Anthony, E.; Sedrati, M.; Harti, A.; Ziane, E. The impact of storms on the morphodynamic evolution of a human-impacted semi-sheltered beach (Agadir Bay, Morocco). *Afr. Earth Sci. J. Afr. Earth Sci.* **2016**, *115*, 32–47. [CrossRef]
26. Daghigh, H.; Khaniki, A.K.; Bidokhti, A.A.; Habibi, M. Prediction of bed ripple geometry under controlled wave conditions: Wave-flume experiments and MIKE21 numerical simulations. *Indian J. Geo Mar. Sci.* **2017**, *46*, 529–537.
27. Gad, F.K.; Hatiris, G.A.; Loukaidi, V.; Dimitriadou, S.; Drakopoulou, P.; Sioulas, A.; Kapsimalis, V. Long-term shoreline displacements and coastal morphodynamic pattern of North Rhodes Island, Greece. *Water* **2018**, *10*, 849. [CrossRef]
28. Belibassakis, K.A.; Karathanasi, F.E. Modelling nearshore hydrodynamics and circulation under the impact of high waves at the coast of Varkiza in Saronic-Athens Gulf. *Oceanologia* **2017**, *59*, 350–364. [CrossRef]
29. Karathanasi, F.; Belibassakis, K.; Anagnostou, C. Simulation of wave field and sediment transport at the Sitia bay. In Proceedings of the 7th National Conference on Management and Improvement of Coastal Zones, Athens, Greece, 20–22 November 2017; pp. 33–42.
30. Lesser, G.R.; Roelvink, J.A.; van Kester, J.A.T.M.; Stelling, G.S. Development and validation of a three-dimensional morphological model. *Coast. Eng.* **2004**, *51*, 883–915. [CrossRef]
31. Brown, J.M.; Davies, A.G. Methods for medium-term prediction of the net sediment transport by waves and currents in complex coastal regions. *Cont. Shelf Res.* **2009**, *29*, 1502–1514. [CrossRef]
32. Roelvink, D.; Reniers, A. *A Guide to Modeling Coastal Morphology*; Advances in Coastal and Ocean Engineering; World Scientific: Singapore, 2011; Volume 12, ISBN 978-981-4304-25-2.
33. Walstra, D.J.R.; Hoekstra, R.; Tonnon, P.K.; Ruessink, B.G. Input reduction for long-term morphodynamic simulations in wave-dominated coastal settings. *Coast. Eng.* **2013**, *77*, 57–70. [CrossRef]
34. Malliouri, S.; Petrakis, D.; Vandarakis, V.; Moraitis, T.; Goulas, G.-A.; Hatiris, G.; Drakopoulou, P.; Kapsimalis, V. A Chronology-Based Wave Input Reduction Technique for Simulations of Long-Term Coastal Morphological Changes: An Application to the Beach of Mastichari, Kos Island, Greece. *Water* **2023**, *15*, 389. [CrossRef]
35. Holthuijsen, L.H.; Booij, N.; Herbers, H.C. A prediction model for stationary, short-crested waves in shallow water with ambient current. *Coast. Eng.* **1989**, *13*, 23–54. [CrossRef]

36. Abbott, M.B. *Computational Hydraulics, Elements of the Theory of Free Surface Flows*, Pitman, ed.; Pitman Publishing Ltd.: London, UK, 1979.
37. Kaergaard, K.; Fredsoe, J. A numerical shoreline model for shorelines with large curvature. *Coast. Eng.* **2013**, *74*, 19–32. [CrossRef]
38. Ashton, A.; Murray, A.B.; Arnoult, O. Formation of coastline features by large-scale instabilities induced by high-angle waves. *Nature* **2001**, *414*, 296–300. [CrossRef]
39. Falque's, A.; Calvete, D. Large-scale dynamics of sandy coastlines: Diffusivity and instability. *J. Geophys. Res.* **2005**, *110*, C03007. [CrossRef]
40. Néelz, S.; Pender, G. *Benchmarking of 2D Hydraulic Modelling Packages*; Science Report SC080035/SR2; Environment Agency: Bristol, UK, 2010.
41. Aernouts, D.; Héquette, A. L'évolution du rivage et des petits-fonds en baie de Wissant pendant le XXe siècle (Pas-de-Calais, France). *Geomorphol. Relief Process. Environ.* **2009**, *1*, 49–64. [CrossRef]
42. Hüttemeyer, P. GIS application for the study of the morphodynamics of the shoreface area of the German Bight: Methods and problems. In *CoastGIS'99: Geomatics and Coastal Environment*; Populus, J., Loubersac, L., Eds.; Serie Actes de Colloques; Ifremer/SHOM: Brest, France, 2000; pp. 222–232.
43. Guillaume, A. *Analyse des Variables Régionalisées*; Doin: Paris, France, 1977; p. 180.
44. Robinson, G. The accuracy of digital elevation models derived from digitized contour data. *Photogramm. Rec.* **1994**, *14*, 805–814. [CrossRef]
45. Guiblin, P.; Rivoirard, J.; Simmonds, E. *Analyse Variographique de Campagnes Acoustiques sur le Hareng Ecossais*; Forum Halieumétrique: Nantes, France, 1996; pp. 93–97.
46. Bourgault, G.; Marcotte, D. Multivariable variogram and its application to the linear model of coregionalization. *Math. Geol.* **1997**, *23*, 899–928. [CrossRef]
47. Anthony, E.J. Wave influence in the construction, shaping and destruction of river deltas: A review. *Mar. Geol.* **2015**, *361*, 53–78. [CrossRef]
48. Zainescu, F.; Vespremeanu-Stroe, A.; Anthony, E.J.; Tatui, F.; Preoteasa, L.; Mateescu, R. Flood deposition and storm removal of sediments in front of a deltaic wave-influenced river mouth. *Mar. Geol.* **2019**, *417*, 106015. [CrossRef]
49. Zainescu, F.; van der Vegt, H.; Storms, J.; Nutz, A.; Bozetti, G.; May, J.-H.; Cohen, S.; Bouchette, F.; May, S.M.; Schuster, M. The role of wind-wave related processes in redistributing river-derived terrigenous sediments in Lake Turkana: A modelling study. *J. Great Lakes Res.* **2023**, *49*, 368–386. [CrossRef]
50. Sadio, M.; Anthony, E.J.; Diaw, A.T.; Dussouillez, P.; Fleury, J.T.; Kane, A.; Almar, R.; Kestenare, E. Shoreline changes on the wave-influenced Senegal River delta, West Africa: The roles of natural processes and human interventions. *Water* **2017**, *9*, 357. [CrossRef]
51. Nmiss, M.; Anthony, E.J.; Mhamed, A.; Ouammou, A. Multi-decadal shoreline change, inherited coastal morphology, and sediment supply in the Souss-Massa littoral cell (Morocco), and a prognosis with sea-level rise. *J. Afr. Earth Sci.* **2022**, *196*, 104672. [CrossRef]
52. Snow, G.C.; Taljaard, S. Water quality in south African temporarily open/closed estuaries: A conceptual model. *Afr. J. Aquat. Sci.* **2007**, *32*, 99–111. [CrossRef]
53. Schallenberg, M.; Larned, S.T.; Hayward, S.; Arbuckle, C. Contrasting effects of managed opening regimes on water quality in two intermittently closed and open coastal lakes. *Estuar. Coast. Shelf Sci.* **2010**, *86*, 587–597. [CrossRef]
54. El Mimouni, A.; Anthony, E.J.; Daoudi, L. Morphological change on a Wadi-influenced beach: Essaouira, Morocco. Géomorphol.-Relief Process. *Géomorphol.-Relief Process. Environ.* **2014**, *20*, 243–250. Available online: https://journals.openedition.org/geomorphologie (accessed on 25 September 2023). [CrossRef]
55. Anthony, E.J. The Human influence on the Mediterranean coast over the last 200 years: A brief appraisal from a geomorphological perspective. *Géomorphologie-Relief Process. Environ.* **2014**, *2014*, 219–226. [CrossRef]